Journal of Materials Science: Materials in Medicine (2019) 30:21
https://doi.org/10.1007/s10856-019-6219-9

BIOMATERIALS SYNTHESIS AND CHARACTERIZATION

Original Research

Exploring the effect of sintering temperature on naturally derived hydroxyapatite for bio-medical applications

S. Aarthy[1] · D. Thenmuhil[1] · G. Dharunya[2] · P. Manohar[1]

Received: 25 May 2018 / Accepted: 9 January 2019 / Published online: 12 February 2019

Abstract

The current work describes the influence of sintering temperatures on biological and mechanical properties of naturally derived hydroxyapatite (HAp). The phase pure hydroxyapatite developed from the goat bone has been obtained by optimizing the calcination temperature from 600–900 °C. Further, HAp calcined at 900 °C was subjected to various sintering temperature (1100–1400 °C). Finally, the influence of sinter temperatures on mechanical (hardness) and biological properties (in vitro bioactivity, MTT and hemocompatibility assays) were ascertained. In respect of biological properties, it came to know that 1300 °C is optimum sinter temperature, which has enhanced apatite growth with the superior cell viability and hemo-compatible behavior. However, sample sintered at 1400 °C delivers maximum hardness. Thus, the hydroxyapatite extracted from goat bone can find better applications in bio-medical engineering as analogous to the existing man-made synthetic materials.

Graphical Abstract

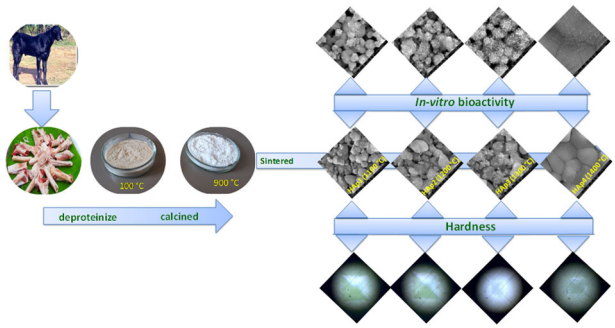

1 Introduction

Sources from bone graft substitution market reveal that the musculoskeletal surgical procedures done annually were counted to be nearly 3 million in global scenario [1]. Probably, the chances for the same at the end of 2020 might be 6.6 million per annum [2]. With the advancement in medical technology, the only existing clinical standard to recover the injured bone is surgical approach. However, the difficulty and scarcity issues of surgical move include long surgical times, donor site morbidity, and limited graft availability associated with allograft and autografts. This offers vast demand for bone grafting materials to solve the current challenging problem [3, 4]. Recently, accomplishment of bone regeneration through tissue engineering strategy is found to have promising future [3]. In this approach, the insertion of scaffolds into the skeletal defect sites favors the bone regeneration similar to normal regeneration.

Different synthetic bio-compatible materials such as polymers, ceramics and composite materials have been employed for bone grafts in modern tissue engineering

✉ P. Manohar
pmano55@yahoo.co.in

[1] Department of Ceramic Technology, Alagappa College of Technology, Anna University, Chennai, TN 600 025, India

[2] Biomaterials Department, CSIR-Central Leather Research Institute, Adyar, Chennai, TN 600 020, India

advancements [4, 5]. Regardless of exhaustive researches, the properties of available scaffolds are still far away from those of natural cortical bones. Ideally, Hydroxyapatite (HAp) has been proven to be a bone-substitute material due to its excellent biocompatibility and osteoconductive properties in addition to the similarity in chemical constitute [$Ca_{10}(PO_4)_6(OH)_2$]. Due to biological importance, HAp received great interest among ceramists since it was identified. Because of the demand and wide scope, various synthetic methodologies have been proven to be a successful approach to develop HAp. However, the present synthetic conditions are failing to reach the commercial value because of their complication in process and high cost.

Apart from the focus to reduce expensiveness of HAp, their mechanical strength necessity as comparable to natural cortical bones is the main demand still persists. Recently, most of the developments are intended to derive the HAp from natural bio-sources such as animal bones, natural rocks and marine species, etc [5–9]. In order to attain simple route to get HAp in unlimited supply with low cost, the naturally calcium enriched materials received much attention of modern ceramist. Though HAp has been obtained from distinguished natural sources, the effect of sintering temperature on mechanical and its biological properties has not been fully described and investigations in this area are still wide open. In this view, very recently, Niakan et al. 2015 [10] studied about certain physical properties such as relative density, Vickers hardness against sintering temperature ranging from 600 to 1000 °C. So, the mechanical properties, biocompatibility, and cytotoxic analysis are still in need to analyze in detail against various sintering temperatures to explore the ultimate utility of animal bones.

Herein, we report the investigation and discussion done on the effect of sintering temperature on the phase purity, morphology, hardness, biocompatibility and cytotoxicity of hydroxyapatite (HAp) derived from goat bone.

2 Experiments

2.1 Materials

Waste goat bones collected from local slaughter house, Chennai, Tamilnadu, India was used as source to extract hydroxyapatite. Sodium hydroxide, polyvinyl alcohol was purchased from Merck, India and double distilled water was used throughout the process.

2.2 Extraction of HAp

Initially, the collected raw bones were cleaned by using large amount of fresh water to make it free from blood impurities. To deproteinize, the washed samples were boiled for 6 h and subsequently treated with 2 M NaOH solution. Further, the deproteinized bones were again washed with distilled water for several times and dried at 100 °C for 24 h. After complete removal of moisture, different amount of samples were subjected to calcination at different temperatures starting from 600 to 900 °C for 5 h at the heating rate of 5 °C/min. The resulted samples were subjected to diffraction analysis and sample (HAp) with no impurity and higher crystallinity (900 °C) was chosen to further sintering process.

2.3 Sintering of HAp

The sample calcinated at 900 °C was ball milled at 300 rpm using tungsten carbide balls for 1 h. The obtained finely divided HAp powder was pelletized using 2% PVA (polyvinyl alcohol) as binder at 150 MPa pressure using cylindrical stainless steel mould by uniaxial pressing. Various temperatures such as 1100, 1200, 1300, and 1400 °C were chosen to sinter the pelletized HAp for 2 h at the heating rate of 5 °C/min. The sintered pellets were labeled as HAp1 (1100 °C), HAp2 (1200 °C), HAp3 (1300 °C) and HAp4 (1400 °C) in all further upcoming discussions.

2.4 Characterization

Thermal analysis (TGA) thermo-gravimetric analysis and differential thermal analysis (DTA) for the raw bone were performed using EXSTAR SII TG/DTA 6300 from ambient temperature to 900 °C. The formation and variation in the phases during various heat treatments were confirmed through Rich Seifert-3000 (Germany) equipped with Copper anode target (Cu Kα radiation of wavelength, $\lambda = 1.54$ Å) powder X-ray diffractometer (XRD). The FTIR spectrum was recorded to analyze the functional group present in the naturally derived Hap using Perkin Elmer 6X FT-IR Spectrometer, (Waltham, Massachusetts, USA) using potassium bromide (KBr) as reference. Surface morphology was analyzed using FEI Quanta FEG 200—High resolution Scanning Electron Microscope in low vacuum mode equipped with Energy dispersive X-ray Spectrometry (EDX) microscope, which helps to evaluate the elemental information of the material from the surface by back-scattered deflection (BSD) system. The Vickers hardness (H_V) of the sintered samples was also determined using Zwick Material prufung hardness testing equipment. Average of five distinguished spot of the sintered samples was used to calculate the hardness value. Bulk density measurement of sintered samples was carried out based on the Archimedes' principle using distilled water as an immersion medium. In vitro bioactivity of the samples was done using Hanks' balanced salt solution obtained from Sigma-Aldrich

as a Simulated Body Fluid (SBF). About 5 ml of Hank's balanced salt solution was taken in four separate plastic vials with lid in which naturally derived HAp pellets sintered at various temperatures (1100–1400 °C) were immersed. It was then placed in incubator at physiological body temperature (37.4 °C) without shaking. After 7 days of incubation period the soaked pellets were taken out and dried at room temperature and cooled in a desiccator. The morphology and elemental composition of the biomineralized samples surface were studied by HRSEM and EDX analysis. The cyto-compatibility of HAp and its sintered derivatives were tested using MTT assay on human osteo sarcoma cell line (MG63). The MG63 cells were cultured using Dulbecco's Modified Eagle's Medium (DMEM) supplemented with 10% Fetal Bovine Serum (FBS) and 1% penicillin, streptomycin, gentamycin solution and were maintained at 37 °C with 5% CO_2. The cells were trypsinized using 1 × Trypsin-EDTA for subculture after it reaches 70% confluence. An approximate count of 5,000 cells/wells were seeded onto 96 well tissue culture plates and incubated for 24 h. HAp and its sintered derivatives of two different concentrations (0.5 mg, 1.0 mg/200 µl) were added to the cells and re-incubated for 24 h. The culture medium was removed after incubation and was replaced with 0.5 mg/ml MTT [3-(4, 5 dimethyl thiazoly-2)-2,5-diphenyl tetrazolium bromide] dissolved in 1 × Phosphate Buffer Saline. The insoluble formazon crystals formed after 4 h of incubation was solubilized in dimethyl sulphoxide (DMSO) and the absorbance was read at 570 nm using Bio-Rad ELISA plate reader. The percentage of cell viability was calculated using the formula,

$$\text{Cell Viability}\,(\%) = [\text{optical density of test sample}/\text{optical density of control}] \times 100$$

The hemocompatible behavior of HAp was tested using human blood collected from healthy volunteers. The red blood cells from heparinized blood were isolated by centrifugation and washed with HEPES buffer (5 mM) containing sodium chloride (150 mM). The ideal concentration of HAp (µg) powder was taken in the centrifuge tubes containing the suspension of 10^8 cells in HEPES buffer (1 ml) and the tubes were incubated at 37 °C for 30 min. After incubation, the tubes were kept for centrifugation to obtain the supernatant. The absorbance of the supernatant was read at 540 nm. The percentage hemolysis of water (positive control) was calculated as 100 %. The percentage hemolysis for HAp was calculated using the formula,

$$\%\ \text{of hemolysis} = \frac{[\text{Absorbance of HAp} - \text{Absorbance of Negative control}]}{[\text{Absorbance of positive control} - \text{Absorbance of negative control}]} \times 100$$

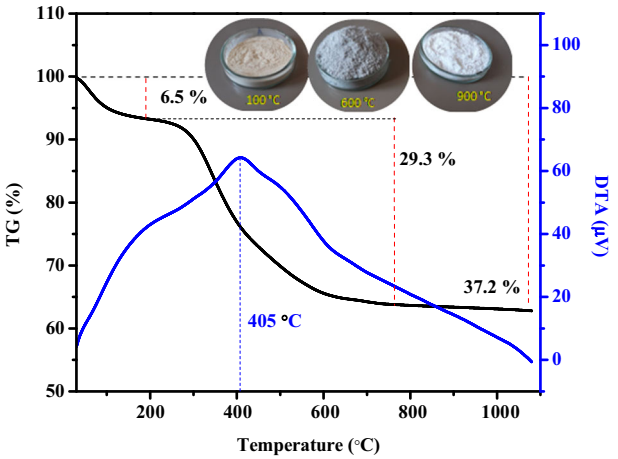

Fig. 1 Thermogram of raw bone sample and inset shows the color variation at different temperatures

3 Results

3.1 TGA analysis

Before subjecting to calcination mentioned in the experimental section, the goat bone sample was subjected to thermal analysis in order to ascertain its thermal behavior. Figure 1 shows the thermogram with two different stages of weight loss. Initially, about 6.5 % weight loss was observed over 30 to 190 °C and subsequent loss of 29.3 % was observed between 190 to 760 °C. Due to the major weight loss between 190 to 760 °C, the DTA curve consequently delivers exothermic peak at 405 °C. Further, there was no notable weight loss after 800 °C in TGA curve. The inset of the diagram shows the direct observation that was noticed before and after calcination. It was found that the as prepared HAp was light yellow in color, whereas the calcined HAp turns to white.

3.2 XRD analysis

Figure 2 illustrates the X-ray diffractogram of the prepared HAp and calcined powders. The major peak appeared at 31.8° corresponding to (2 1 1) lattice plane of hydroxyapatite and the same was found to be present in all the samples irrespective of the thermal treatment. Further, even after high temperature sintering, the samples show the existence of hydroxyapatite phases which are similar to the pattern of JCPDS 09-0432 (Fig. 3). Further, the d spacing of major peak and calculated crystalline sizes by applying Scherrer's method [11] are listed in Table 1.

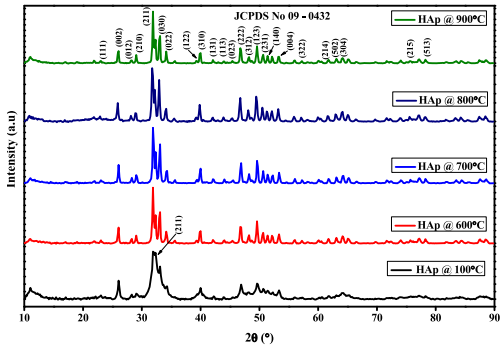

Fig. 2 XRD patterns of raw hydroxyapatite (100 °C) and hydroxyapatite calcined at different temperatures

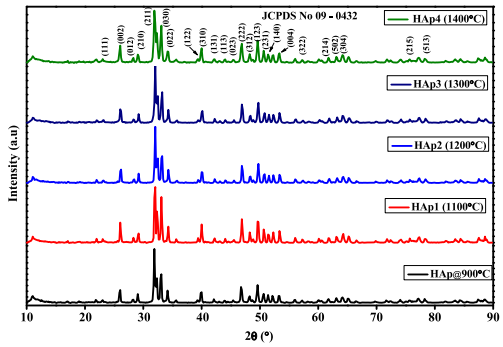

Fig. 3 XRD patterns of calcined hydroxyapatite (900 °C) and conventionally sintered hydroxyapatite at different temperatures

Table 1 '*d*'-spacing values and crystallite sizes of HAp at different temperatures

Samples calcined/sintered at (°C)	Crystallite size (nm)	'*d*' Spacing (211)
100	7.6	2.788
600	15.1	2.719
700	15.1	2.714
800	22.7	2.714
900	22.7	2.714
1100	22.7	2.705
1200	22.7	2.702
1300	22.7	2.702
1400	22.9	2.712

3.3 FTIR analysis

Figures 4a, b illustrates the FTIR spectra of the calcined and sintered HAp powders. The peaks appeared at 962 and 474 cm^{-1} confirms the presence of phosphate groups, the vibrations of which are associated with the symmetric stretching mode respectively [12–14]. However, the asymmetric stretching of the same has been observed from 1013 to 1103 cm^{-1} with a broad peak respectively. Further, the bending bands of the phosphate (O-P-O) groups have been

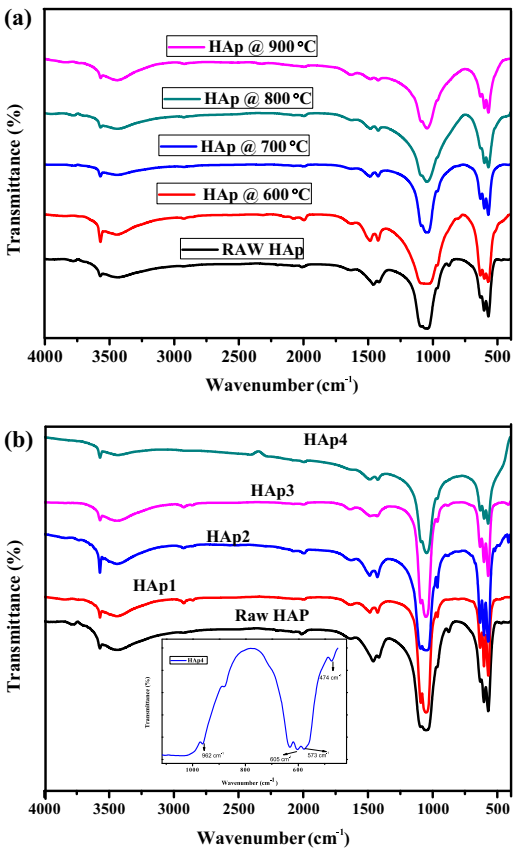

Fig. 4 FTIR Spectra of **a** raw and calcined HAp's and **b** raw and sintered HAp's

observed at 573 and 605 cm^{-1} [8, 11, 15]. The sharp and less intense bands observed at 3568 and 3691 cm^{-1} corresponds to the vibration of water molecules in IR region.

3.4 Vickers hardness

Figure 5 illustrates the Vickers hardness (H_V) values of the samples sintered at different temperatures. The average H_V of the naturally derived HAp increases with increase in sintering temperature. Initially, the H_V value was calculated to be 164.3 MPa at 1100 °C (HAp1), however it became to increases as 169.5 MPa at 1200 °C (HAp2), 245.3 MPa at 1300 °C (HAp3) and finally reaches the maximum of 301.3 MPa at 1400 °C (HAp4).

3.5 SEM and particle size analysis

Figure 6 illustrates the SEM images and EDX profiles of the raw and calcined (900 °C) HAp samples. The raw HAp delivers rough surface and irregular morphology with various particle sizes as specified in Fig. 6a, c. However, the SEM image of the calcined HAp presented in Fig. 6b, d shows distinguished morphology compared to raw HAp, in which the particle surface was found to be smooth along

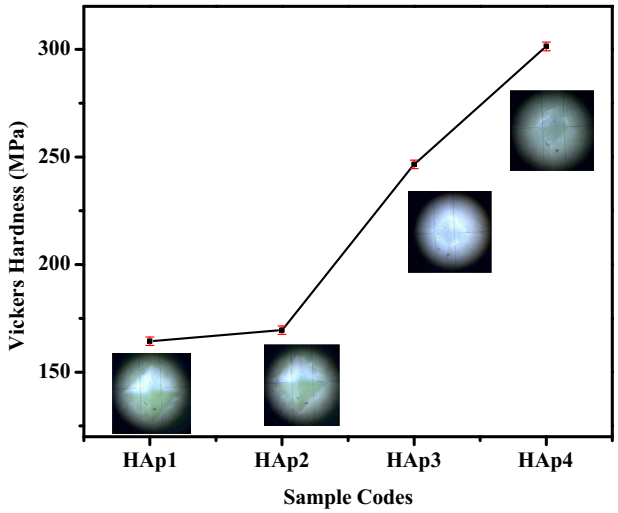

Fig. 5 Vickers hardness of sintered samples

with discrete plate like appearance with average particle size of 1 µm. The elemental profiles obtained from EDX results shown in Fig. 6e–f confirmed that the HAp owns the Ca/P ratio as 1.64, which is nearly equivalent to the reported value 1.67. Further, the calcination yields a significant outcome in the particle size distribution. The average particle size distribution of the HAp calcined at 900 °C (Fig. 7b) was found to be about 1 µm (D_{50}), which is comparatively lower than the raw samples which has a wide range of particle size distribution ranging from 1.5 µm to 262 µm with D_{50} value is of 16 µm (Fig. 7a). Figure 8 illustrates the SEM images of sintered HAp at various temperatures ranging from 1100 to 1400 °C. After sintering, the HAp morphology shows significant transformations, which are presented in the Fig. 8a–d. The SEM images of the sintered HAps clearly display the grain growth morphology and clear grain boundaries.

3.6 In vitro bio-activity evaluation

Evaluation of the bioactivity of the naturally derived HAp is highly essential to move towards the application. Subsequently, the prepared HAp samples were incubated in SBF for 7 days and were used to evaluate the growth of apatite like layer over the surface through microscopic analysis. The formations of apatite over the surface of sintered samples at different temperatures are shown in Fig. 9a–d. The observation shows that the sintered samples support the growth of hydroxyapatite and so are biocompatible in nature. The HAp samples sintered at temperatures 1100 and 1400 °C could not favor equivalent growth as like the samples sintered at 1200 and 1300 °C. On the other hand, the sample sintered at 1300 °C (HAp3), delivers excellent and uniform growth. The grown-up apatite's forms wrinkle like structure, which was comparably high in sample HAp3 (1300 °C) than HAp2 (1200 °C). Further, the corresponding elemental profiles are also given in the Fig. 9.

3.7 Cytotoxic evaluation

The cyto-compatibility of HAp and its sintered particles in MG63 was studied using MTT assay and the results are shown in Fig. 10a–f. The cell morphology as observed from the results remains intact in the both HAp and its sintered derivatives treated cells. Figure 10ii shows the % cell viability of the naturally derived HAp and its sintered particles (HAp1–HAp4) with two varying concentrations.

3.8 Hemocompatible behavior

The hemocompatible analysis of prepared HAp3 is essential towards bio-medical tissue engineering or bone replacement applications. Figure 11 shows the percentage hemolysis behavior of the HAp3 at different concentrations (10, 25, 50, 75, 100, 200 µg). The result illustrates the hemolysis percentage varies as 2.37, 2.93, 3.56, 3.95, 4.3, and 4.56% with increase in the concentration of HAp3 (10, 25, 50, 75, 100, 200 µg), respectively.

4 Discussions

The weight loss of 6.5% occurred over 30–190 °C is associated with the evaporation of both physisorbed and chemisorbed water molecules. Further, the degradation with subsequent weight loss of 29.3% that occurred over 190–760 °C ascribes to the combustion of volatile matters of bone, which has also been supported from the exothermic peak of DTA curve at 405 °C (Fig. 1). Similar results were also independently observed by Younesi et al, and Krzesinska et al. at comparable temperature series [16, 17]. The combustion of volatile matter is owing to disintegration of organic substances of bone, which burned out in air to yield calcium phosphate powder. Consequently, the extracted calcium phosphate was subjected to various calcination temperatures starting from 600 to 900 °C to ascertain the exact temperature required for the formation of hydroxyapatite phases. Further, the inset shows the different color shades of the HAp from pale yellow to white with respect to calcination temperature. Appearance of light yellow color of the as prepared HAp is due to the presence of organic matrix such as protein and collagen. Later, at 600 °C the dark grey color is associated with the incomplete removal organic matrix. Finally, white color is evident for the complete removal of organic compositions.

Figure 2 delivers the variation in the complete formation of HAp phase's with increase in temperature. The proportionate growth of phases was achieved only at high

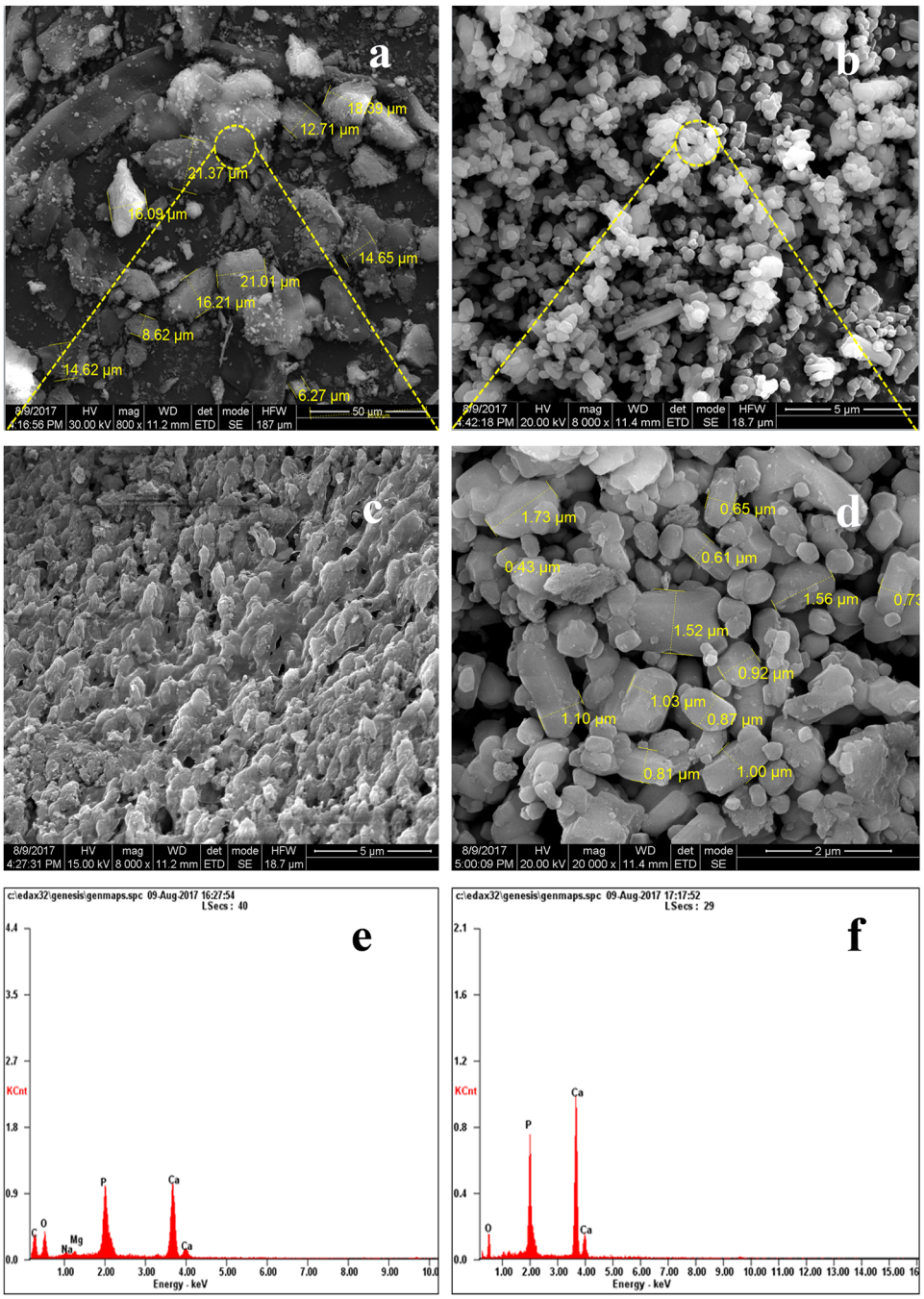

Fig. 6 **a**, **b** SEM micrographs of raw and calcined HAp, **c**, **d** magnified image of raw and calcined HAp, and **e**, **f** EDX profile of raw and calcined HAp

temperature, which became narrow and sharper. It was found that the formation of pure phases of HAp was completely achieved at 900 °C. The obtained results are in good agreement with those samples which are subjected to thermal treatment as in earlier reports [8, 16, 18] and JCPDS No 09-0432. Thus, the HAp powder calcinated at 900 °C was chosen for further sintering temperatures starting from 1100 to 1400 °C. The diffractogram results (Fig. 3) of the sintered samples delivers no phases of α-tri-calcium phosphate, β-tri-calcium-phosphate, tetra-calcium phosphate or calcium oxide. These results support the formation pure HAp in crystalline form without any secondary phases. Generally, the preparation of HAp using calcium and phosphate precursors through thermal treatment results in secondary phases of calcium phosphates, which disturbs the crystallinity of HAp. The obtained results are in good accordance with various typical HAp powders that were prepared from various bone sources [19–22]. The major peaks at 31.8° and 25.8° corresponds to (2 1 1) and (0 0 2) planes of HAp as referred by JCPDS files (09-0432) [22–25]. The XRD

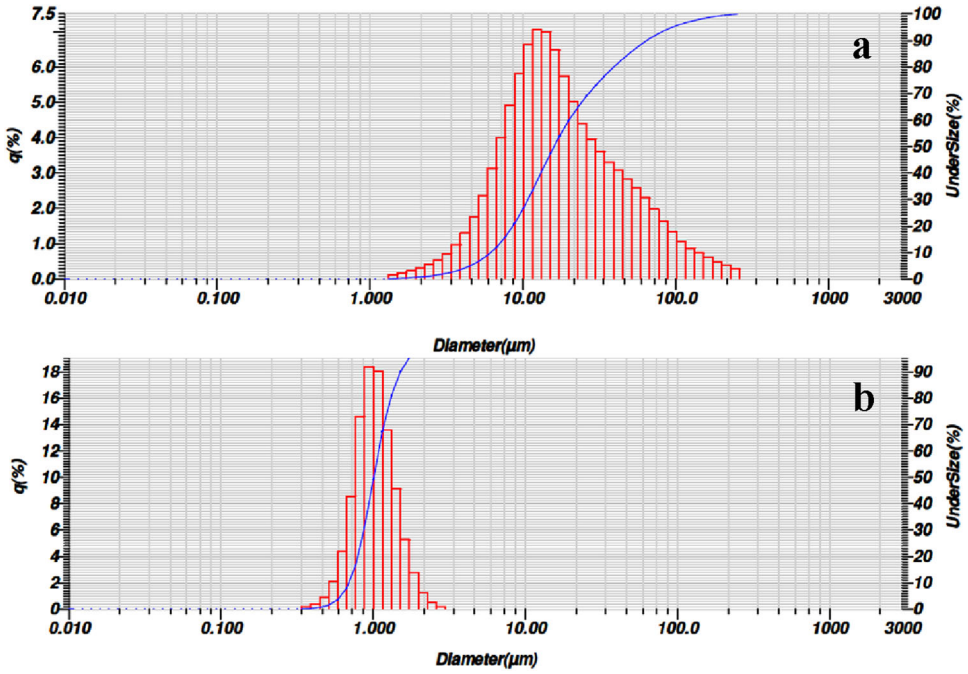

Fig. 7 Particle-size distributions of **a** raw HAp and **b** calcined HAp at 900 °C

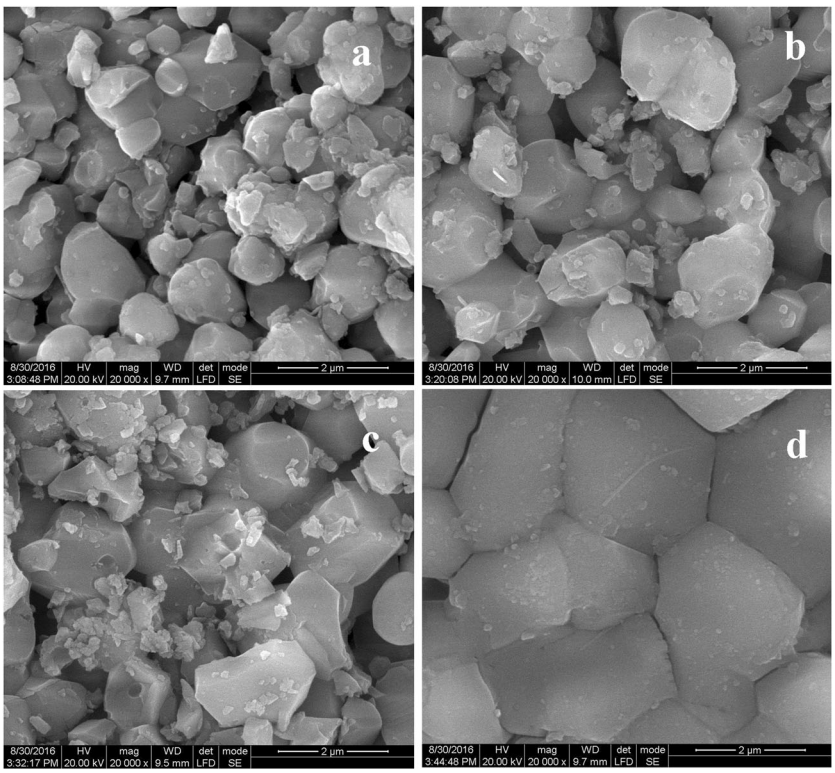

Fig. 8 SEM micrographs of **a** HAp1, **b** HAp2, **c** HAp3, and **d** HAp4

patterns of sintered HAps from1100 to 1400 °C shows fine crystalline particles of hexagonal system with space group of P63/m [16, 26].

Figure 4 conveys the complete information about the functional groups of HAp. However, some additional peaks at 3568 and 3691 cm^{-1} are due to the presence of moisture in the crystal lattices [26]. Further, the peaks observed at 880, 1414 and 1462 cm^{-1} are due to presence of carbonate ions which might have appeared from the atmospheric carbon dioxide. Thus, the FTIR analysis of the HAp confirms that the existence of hydroxyapatite along with functional constituents without other impurities.

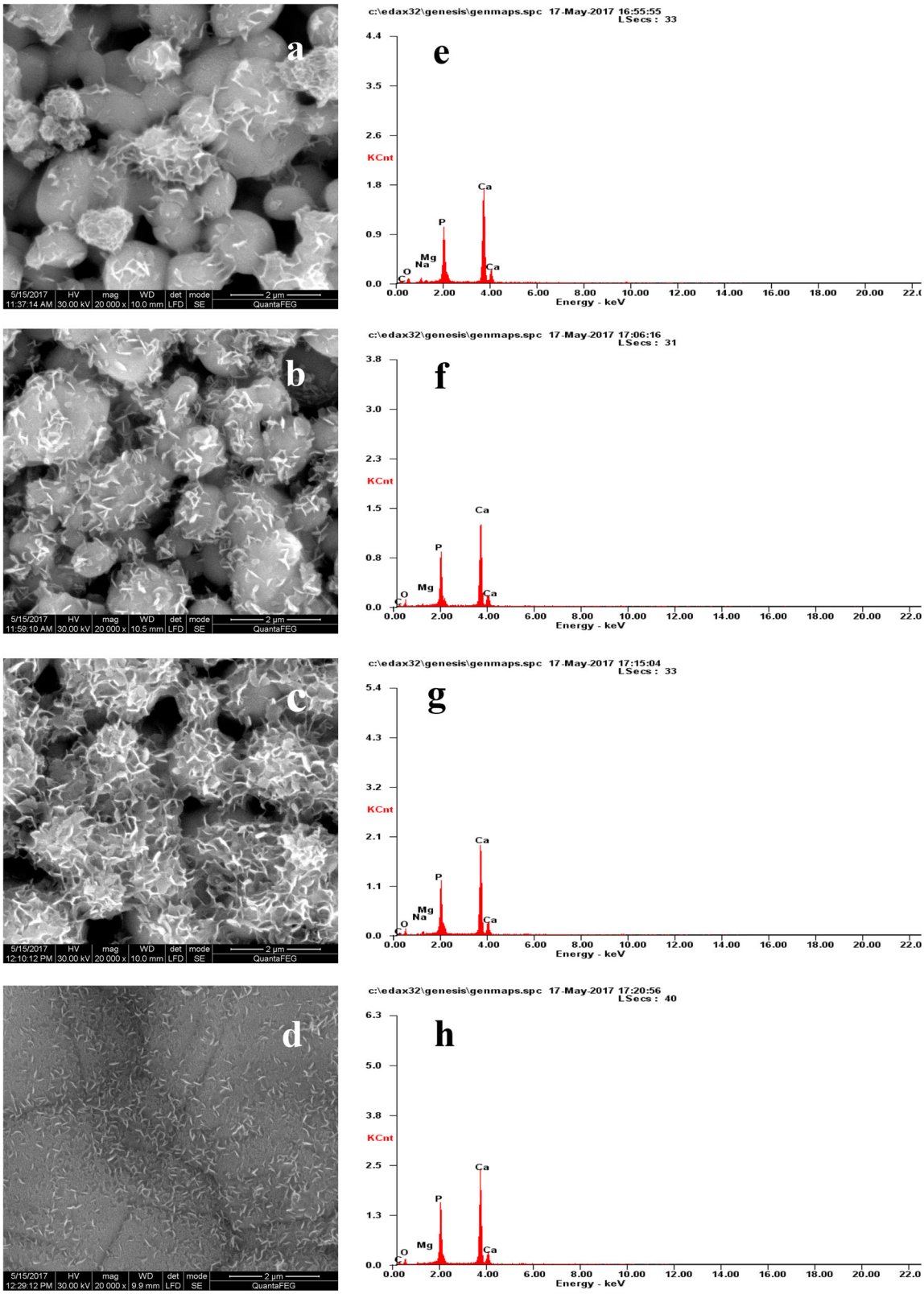

Fig. 9 SEM micrographs **a**–**d** and EDX results **e**–**h** of HAp1, HAp2, HAp3, and HAp4, respectively, after 7 days incubated in SBF solution

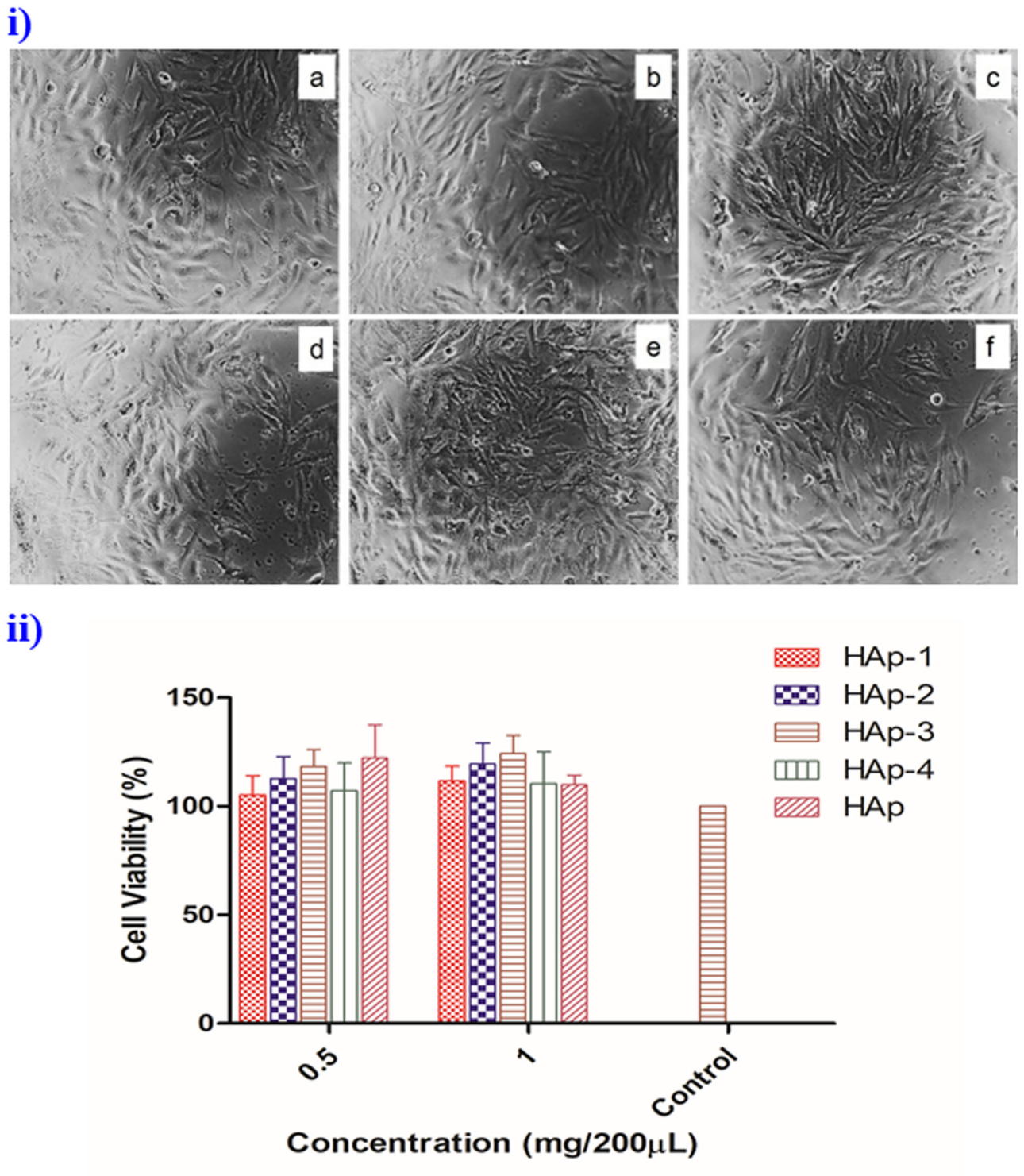

Fig. 10 (i) **a**–**d** Microscopic images of HAp1 to HAp4, respectively, **e** calcined HAp (900 °C), and **f** control and (ii) Cell viability profile for HAp at 0.5 and 1.0 mg/200 µl

The H_V value obtained in the present work (Fig. 5) is comparably high than that of sintered porous HAp derived from bovine bone reported elsewhere. Niakan et al. 2015 reported the sintering behavior of hydroxyapatite up to 1000 °C. It is known that, the hardness increases with increasing sintered density [10]. Thus, the H_V of HAp3 sintered at 1300 °C is also found to be comparatively high (246.5 MPa) than the previous report, which is also

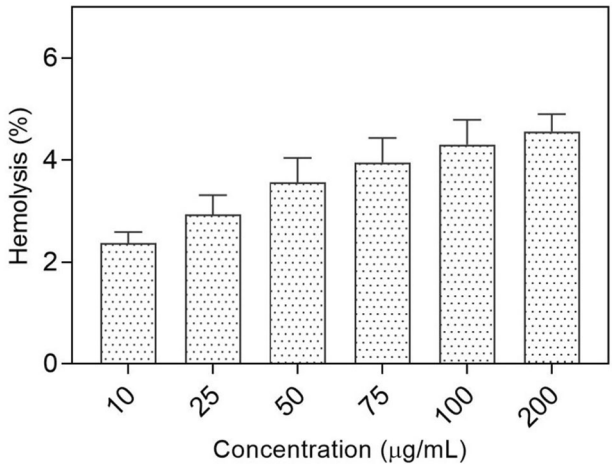

Fig. 11 % hemolysis of the HAp3 at different concentrations

associated with superior biocompatibility as confirmed in our results.

In Fig. 6a–d, the typical difference in morphology before and after calcination such as formation of the discrete plate like particles and smooth surface is due to the removal of organic residuals over the natural bone when subjected to high temperature [16]. The results obtained in SEM are in accordance with those of results supported by average particle size distribution. Figure 8 illustrates the SEM images of sintered HAp at various temperatures from 1100 to 1400 °C. After sintering, the HAp morphology shows significant transformations, which are presented in the Fig. 8a–d. The sintered HAP delivers discrete grain structure with clear grain boundary morphology. The naturally existing inter connected porous grain structures became more closer to each other, which ultimately leads to the formation of defined crystalline grain structure of HAp [7, 25, 27, 28]. Thus, sample HAp4 sintered at 1400 °C brings denser and smooth surface with separate grain structures and grain boundaries.

Figure 9 a–d exemplifies the in vitro bioactivity results for the sintered HAp's. The wide variations appeared in the growth of apatite on the surface of the sintered pellets are probably due to the presence of excess porous structure in the sample HAp1 and highly dense grain structure in sample HAp4. However, phenomenal growth in HAp3 is attributed due to the presence of optimum surface along with pores and grain structure that suited for the nucleation followed by spontaneous precipitation and growth of apatite particulates. [13, 27, 29]. So it can be concluded that compared to dense HAp, the porous and extended surfaces of HAp have great influence in apatite's growth. The results evidently suggest that HAp sintered at 1300 °C has better apatite growth compared to other sintering temperature. Figure 9e–h reveals the presence of very low proportion of Na, Mg and C in addition to calcium and phosphorous ions [30]. This result is evident for the formation of biomineralized sample from the chemical reactions between sintered HAps and SBF.

The results evidently confirmed that HAp particles derived from goat bone and its sintered derivatives had no significant toxicity towards cell growth. The cells exposed to different concentrations (0.5 and 1.0 mg/200 µl) of HAp and its sintered derivatives were found to exhibit the cell viability around 100% as depicted in Fig. 10. This clearly indicates that HAp and its sintered particles at these concentrations were nontoxic to the MG63 cells without affecting the cell growth [30]. In addition, cell proliferation was observed to be higher for the particles sintered at 1300 °C (HAp3) compared to control and other samples. Interestingly, HAp3 samples exhibit more bioactivity, as confirmed in SBF immersion studies.

The hemocompatibility result presented in the Fig. 11 for the prepared HAp3 does not show any toxicity in application. Generally, the biological implants and replacements should deliver hemolysis less than 5%, however our observed data delivers only 4.5%, which shows reliability and validates as a promising material for application [23].

5 Conclusions

In summary, the waste bones used as hydroxyapatite precursor, were subjected to various sintering temperature to ascertain its hardness and biocompatibility nature. The analytical results from diffraction analysis confirm the formation of phase pure hydroxyapatite. The grain growth morphology was exemplified with respect to different sintering temperatures. SBF immersion studies confirm that the 1300 °C is the optimum temperature that favors the formation of biomineralized apatite on the HAp surfaces. Further, MTT cytocompatibility assay result indicates the excellent growth and proliferation of MG63 cells with enhanced viability similar to control cells. In addition, the resulted hemolysis (%) was less than 5%, which is in acceptable ASTM limits. Therefore, our studies on bio-derived HAp can find suitable applications in bio-medical engineering. Thus, the natural goat bones can be suited for various bio-medical applications such as tissue engineering and bone replacement [31, 32].

Compliance with ethical standards

Conflict of interest The authors declare that they have no conflict of interest.

Publisher's note: Springer Nature remains neutral with regard to jurisdictional claims in published maps and institutional affiliations.

References

1. Wang Q, Chen C, Liu W, He X, Zhou N, Zhang D et al. Levofloxacin loaded mesoporous silica microspheres/nano-hydroxyapatite/polyurethane composite scaffold for the treatment of chronic osteomyelitis with bone defects. Sci Rep. 2017;2:41808.
2. Lee DJ, Lee YT, Zou R, Daniel R, Ko CC. Polydopamine-laced biomimetic material stimulation of bone marrow derived mesenchymal stem cells to promote osteogenic effects. Sci Rep. 2017;7:12984.
3. Szczes A, Yan Y, Chibowski E, Hołysz L, Banach M. Properties of natural and synthetic hydroxyapatite and their surface free energy determined by the thin-layer wicking method. Appl Surf Sci. 2018;434:1232–8.
4. Mansour SF, El-Dek SI, Ahmed MK. Physico-mechanical and morphological features of zirconia substituted hydroxyapatite nano crystals. Sci Rep. 2017;7:43202.
5. Mondal S, Pal U, Dey A. Natural origin hydroxyapatite scaffold as potential bone tissue engineering substitute. Ceram Int. 2016;42:18338–46.
6. Heidari F, Bahrololoom ME, Vashaee D, Tayebi L. In situ preparation of iron oxide nanoparticles in natural hydroxyapatite/chitosan matrix for bone tissue engineering application. Ceram Int. 2015;41:3094–100.
7. Lowe B, Venkatesan J, Anil S, Shim MS, Kim SK. Preparation and characterization of chitosan-natural nano hydroxyapatite-fucoidan nanocomposites for bone tissue engineering. Int J Biol Macromol. 2016;93:1479–87.
8. Chakraborty R, Roy Chowdhury D. Fish bone derived natural hydroxyapatite-supported copper acid catalyst: taguchi optimization of semibatch oleic acid esterification. Chem Eng J. 2013;215:491–9.
9. Brzezińska-Miecznik J, Haberko K, Sitarz M, Bućko MM, Macherzyńska B, Lach R. Natural and synthetic hydroxyapatite/zirconia composites: a comparative study. Ceram Int. 2016;42:11126–35.
10. Giraldo-Betancur AL, Espinosa-Arbelaez DG, del Real-López A, Millan-Malo BM, Rivera-Muñoz EM, Gutierrez-Cortez E et al. Comparison of physicochemical properties of bio and commercial hydroxyapatite. Curr Appl Phys. 2013;13:1383–90.
11. Lombardi M, Palmero P, Haberko K, Pyda W, Montanaro L. Processing of a natural hydroxyapatite powder: from powder optimization to porous bodies development. J Eur Ceram Soc. 2011;31:2513–8.
12. Niakan A, Ramesh S, Ganesan P, Tan CY, Purbolaksono J, Chandran H et al. Sintering behaviour of natural porous hydroxyapatite derived from bovine bone. Ceram Int. 2015;41:3024–9.
13. Swain SK, Bhattacharyya S. Preparation of high strength macroporous hydroxyapatite scaffold. Mater Sci Eng: C. 2013;33:67–71.
14. Mondal S, Mondal B, Dey A, Mukhopadhyay SS. Studies on processing and characterization of hydroxyapatite biomaterials from different bio wastes. J Miner Mater Charact Eng. 2012;11:55.
15. Akram M, Ahmed R, Shakir I, Ibrahim WA, Hussain R. Extracting hydroxyapatite and its precursors from natural resources. J Mater Sci. 2014;49:1461–75.
16. Ooi CY, Hamdi M, Ramesh S. Properties of hydroxyapatite produced by annealing of bovine bone. Ceram Int. 2007;33:1171–7.
17. Younesi M, Javadpour S, Bahrololoom ME. Effect of heat treatment temperature on chemical compositions of extracted hydroxyapatite from bovine bone ash. J Mater Eng Perform. 2011;20:1484–90.
18. Krzesińska M, Majewska J. Physical properties of continuous matrix of porous natural hydroxyapatite related to the pyrolysis temperature of animal bones precursors. J Anal Appl Pyrolysis. 2015;116:202–14.
19. Hui P, Meena SL, Singh G, Agarawal RD, Prakash S. Synthesis of hydroxyapatite bio-ceramic powder by hydrothermal method. J Miner Mater Charact Eng. 2010;9:683.
20. Yeong KC, Wang J, Ng SC. Mechanochemical synthesis of nanocrystalline hydroxyapatite from CaO and $CaHPO_4$. Biomaterials. 2001;22:2705–12.
21. Tlotleng M, Akinlabi E, Shukla M, Pityana S. Microstructures, hardness and bioactivity of hydroxyapatite coatings deposited by direct laser melting process. Mater Sci Eng: C. 2014;43:189–98.
22. Raya I, Mayasari E, Yahya A, Syahrul M, Latunra AI. Synthesis and characterizations of calcium hydroxyapatite derived from crabs shells (Portunus pelagicus) and its potency in safeguard against to dental demineralizations. Int J Biomater. 2015;469176:8.
23. Sunil BR, Jagannatham M. Producing hydroxyapatite from fish bones by heat treatment. Mater Lett. 2016;185:411–4.
24. Mukherjee S, Nandi SK, Kundu B, Chanda A, Sen S, Das PK. Enhanced bone regeneration with carbon nanotube reinforced hydroxyapatite in animal model. J Mech Behav Biomed Mater. 2016;60:243–55.
25. Zhao XY, Zhu YJ, Chen F, Lu BQ, Wu J. Nanosheet-assembled hierarchical nanostructures of hydroxyapatite: surfactant-free microwave-hydrothermal rapid synthesis, protein/DNA adsorption and pH-controlled release. CrystEngComm. 2013;15:206–12.
26. Kusrini E, Sontang M. Characterization of x-ray diffraction and electron spin resonance: Effects of sintering time and temperature on bovine hydroxyapatite. Radiat Phys Chem. 2012;81:118–25.
27. Haberko K, Bućko MM, Brzezińska-Miecznik J, Haberko M, Mozgawa W, Panz T et al. Natural hydroxyapatite—its behaviour during heat treatment. J Eur Ceram Soc. 2006;26:537–42.
28. Murugan R, Ramakrishna S, Rao KP. Nanoporous hydroxycarbonate apatite scaffold made of natural bone. Mater Lett. 2006;60:2844–7.
29. Duan S, Feng P, Gao C, Xiao T, Yu K, Shuai C et al. Microstructure evolution and mechanical properties improvement in liquid-phase-sintered hydroxyapatite by laser sintering. Materials. 2015;8:1162–75.
30. Radha G, Balakumar S, Venkatesan B, Vellaichamy E. Evaluation of hemocompatibility and in vitro immersion on microwave-assisted hydroxyapatite–alumina nanocomposites. Mater Sci Eng: C. 2015;50:143–50.
31. Khoo W, Nor FM, Ardhyananta H, Kurniawan D. Preparation of natural hydroxyapatite from bovine femur bones using calcination at various temperatures. Procedia Manuf. 2015;2:196–201.
32. Trinkūnaitė-Felsen J, Žalga A, Kareiva A. Characterization of naturally derived calcium compounds used in food industry. Chemija. 2012;23:76–85.